Electronic Supplementary Information

Structure and Reactivity of a Seven-coordinate Ruthenium Acylperoxo Complex

Rui Wang[ab], Yunling Pan[ac], Sushan Feng[ad], Chenyi Liang[ab], Jianhui Xie[c], Tai-Chu Lau[e] and Yingying Liu*[a]

[a] Institute of Intelligent Machines, Hefei Institutes of Physical Science, Chinese Academy of Sciences, Hefei 230031, P. R. China. Email: yyliu@iim.ac.cn

[b] Uinversity of Scinece Island Branch, Graduate School of USTC, Hefei 230026, P. R. China.

[c] Anhui Province Key Laboratory of Advanced Catalytic Materials and Reaction Engineering, School of Chemistry and Chemical Engineering, Hefei University of Technology, Hefei 230009, P. R. China.

[d] Institutes of Physical Science and Information Technology, Anhui University, Hefei 230601, P. R. China.

[e] Department of Chemistry, City University of Hong Kong, Kowloon Tong, Hong Kong, P. R. China.

Index *Page*

Materials. All organic substrates were purchased either from Aldrich, Aladdin or TCI Chemicals and were purified before use according to the literature.[1] All solvents, such as acetone, acetonitrile, dichloromethane and n-hexane, were in HPLC grade and further purified by following literature methods before use.[1] H*m*CPBA (*m*-chloroperbenzoic acid) was purified before use according to the literature.[1] D_2O (Aldrich, 99 atom % D), $H_2{}^{18}O$ (Aldrich, 97 atom % ^{18}O) and $(NH_4)_2Ce(NO_3)_6$ (Aldrich, Ce(IV)) were used as received. Deuterated substrates, such as xanthene-d_2 and 9,10-dihydroanthracene-d_4 (DHA-d_4) were synthesized according to the the literature.[2] $[Ru^{III}(bdpm)(pic)_2]^+$ (**Ru^{III}**, H_2bdpm = [2,2'-bipyridine]-6,6'-diylbis(diphenylmethanol); pic = 4-picoline) was prepared according to reported procedures.[3] Other chemicals were used as purchased.

Instrumentation. ^{1}H NMR spectra were obtained from a Bruker JNM-ECZ600R/S1 Superconducting Fourier Nuclear Magnetic Resonance Spectrometer. The chemical shifts (δ, ppm) were reported with reference to tetramethylsilane (TMS). Electrospray ionization mass spectrometry (ESI/MS) was carried out on a SCIEX TRIPLE QUAD 3500 mass spectrometer. The analyte solution was continuously infused with a syringe pump at a constant flow rate of 10 μLmin^{-1} into the pneumatically assisted electrospray probe with nitrogen as the nebulizing gas. Kinetics experiments were carried out by using an Agilent 8453 diode-array spectrophotometer. The temperature of the solutions was maintained with an IKEA HRC 2 temperature controller connected to a circulating bath. Gas chromatographic (GC) analyses were performed on a Shimadzu GC2010 Pro FID gas chromatograph equipped with a HP-5 (30 m × 0.25 mm i.d.) capillary column. GC/MS measurements were carried out on a Thermo Scientific Trace 1300 GC interfaced to a ISQ 7000 MS equipped with a TG-5SILMS (30 m × 0.25 mm i.d.). IR spectra were recorded as KBr pellets on a PerkinElmer Spectrum100 FT-IR spectrophotometer at 4 cm^{-1} resolution. Cyclic voltammetry was performed on a CH Instruments Electrochemical Workstation CHI660E. A glassy carbon working electrode, an Ag/AgCl reference electrode, and a Pt wire counter electrode were used. MBRAUN UNILab Pro glovebox was used in the synthesis of unstable compounds.

Kinetics. All reactions were run in 1.0 cm UV cuvette at 0 ºC to 15 ºC under argon and followed by monitoring UV-Vis spectral changes of the reaction solutions under pseudo-first-order conditions. Pseudo-first-order rate constants, k_{obs}, were obtained by nonlinear least-square fits of A_t vs t according to the equation $A_t = A_\infty + (A_0 - A_\infty)\exp(-k_{obs}t)$, where A_0 and A_∞ are the initial and final absorbance at 472 nm, respectively. Reactions were run at least in triplicate,

and the data reported are the average of the reactions. $[Ru^{IV}(bdpm)(pic)_2(mCPBA)]^+$ (**Ru^{IV}-*m*CPBA**) was generated in situ by adding 1.5 equiv. of H*m*CPBA to **Ru^{III}** (3 mM) in acetone. Then substrates were added when the UV absorbance at 472 nm reached a minimum value.

Oxidation of Substrates. Typically, H*m*CPBA (1 mM) was added to a solution of **Ru^{III}** (1 mM) in acetone at 20 °C under argon. After one minute the substrate is added to the above reaction. After stirring for 2 h, bromobenzene (5 mM) was then added as an internal standard, and the mixture was analyzed by GC and GC/MS. Products were identified by comparing with authentic samples. Product yields were determined by comparing peak areas of the reaction solutions with that of bromobenzene as an internal standard. Reactions were run at least in triplicate, and the data reported are the average of the reactions. Yields were calculated based concentration of ruthenium. The ruthenium products formed in the reaction of **Ru^{IV}-*m*CPBA** with substrates were analyzed by ESI/MS. In those the reactions, **Ru^{III}** species were produced as a major product.

^{18}O labelling experiment. For oxidation by **Ru^{IV}-*m*CPBA**, 40 μL of $H_2{}^{18}O$ was added to an acetone solution of **Ru^{IV}-*m*CPBA** (1 mM), which was prepared by directly dissolving isolated **Ru^{IV}-*m*CPBA** solid in 0.5 mL acetone. Substrates were added after 30 s. The sample was diluted before MS analysis. For oxidation by $(NH_4)_2[Ce(NO_3)_6]$ [Ce(IV)], 40 μL of $H_2{}^{18}O$ was added to a solution (acetone/H_2O, v:v 10:1, 0.5 mL) of **Ru^{III}** (1.5 mM)/Ce(IV) (2 equiv.). Substrates were added after 30 s.

X-ray Structure Determination. Crystals of **Ru^{IV}-*m*CPBA**$[PF_6]$ (CCDC No.: 2291470) were obtained by standing a mixture of n-hexane and acetone solution of **Ru^{III}**/H*m*CPBA(3 equiv.) at −30 °C for 1 day. Crystal data and experimental details are listed in Table S1. Selected bond angles and bond lengths are given in Table S2. Crystals of suitable size coated with paratone-N and mounted on a nylon cryoloop were used for X-ray diffraction analysis. X-ray diffraction data were collected using ω-scan mode at 105 K on a Rigaku Oxford Diffraction XtaLAB PRO 007HF (Cu) diffractometer equipped with Dectris PILATUS 200K detector and Oxford Cryostream 800 cooling system using Cu-Kα radiation (λ = 1.54178 Å). A data collection strategy to ensure maximum completeness and redundancy was determined using CrysAlisPro.[4] Data processing was done using CrysAlisPro and a multi-scan absorption correction applied using the SCALE3 ABSPACK scaling algorithm.[5] The structure was solved via intrinsic phasing

methods using SHELXT[6] and refined using SHELXL[7] in the Olex2[8] graphical user interface. The final structural refinement included anisotropic temperature factors on all non-hydrogen atoms. All hydrogen atoms were attached via the riding model at calculated positions and these are participated in the calculation of final R-indices. The automatic "solvent masking procedure" present in OLEX2 was used to mask the solvent molecules present in these structures.[8-10] A solvent mask was applied in Olex2 to two regions of highly disordered residual electron density presumed to be 1 and 0.75 interstitial acetone molecules.

Synthesis.

$[Ru^{IV}(bdpm)(pic)_2(mCPBA)](PF_6)$ (**Ru^{IV}-*m*CPBA**$[PF_6]$): In a glovebox, 3 equiv. of H*m*CPBA (1.9 mg, 0.011 mmol) was dissolved into 0.5 mL acetone then added to a solution of $[Ru^{III}(bdpm)(pic)_2](PF_6)$ (3.5 mg, 0.0037 mmol) in 1 mL acetone at −30 °C. The color of the solution changed from brown to red after shaking for 30 s. The resulting solution was mixed with 10 mL cold n-hexane to form a cloudy mixture and allowed to stand at −30 °C for 1 day to afford red brown crystals which were suitable for X-ray diffraction analysis. Yield: 2.7 mg (66%).^{1}H NMR (600 MHz, Acetone-D_6) δ 9.15 (d, J = 7.8 Hz, 2H), 8.55 (t, J = 7.8 Hz, 2H), 8.00 (d, J = 6.1 Hz, 1H), 7.88 (d, J = 5.8 Hz, 4H), 7.81 (d, J = 5.8 Hz, 1H), 7.70 (d, J = 8.0 Hz, 1H), 7.58 (t, J = 8.2 Hz, 1H), 7.33 (d, J = 7.7 Hz, 2H), 7.17 (t, J = 7.3 Hz, 4H), 7.05 (t, J = 7.6 Hz, 8H), 6.86 (d, J = 7.7 Hz, 8H), 6.72 (d, J = 5.7 Hz, 4H), 2.30 (s, 6H). ESI/MS in acetone: m/z = 977 (M^+) (please refer to Figure S2).

$[Ru^{IV}(bdpm)(pic)_2(mCPBA)](ClO_4)$ (**Ru^{IV}-*m*CPBA**$[ClO_4]$): The method is similar to that of **Ru^{IV}-*m*CPBA**$[PF_6]$ but using $[Ru^{III}(bdpm)(pic)_2](ClO_4)$ as starting material. $[Ru^{III}(bdpm)(pic)_2](ClO_4)$ was prepared by adding a saturated solution of $NaClO_4$ to a MeCN solution of $[Ru^{III}(bdpm)(pic)_2](PF_6)$ (20 mg, 5 mL). The product was collected as precipitation and dried under vacuum.

Table S1. Crystal data and structure refinement details for **Ru^{IV}-*m*CPBA**[PF_6]·0.5C_3H_6O (CCDC No.: 2291470).

Empirical formula	$C_{56.5}H_{47}ClF_6N_4O_{5.5}PRu$
Formula weight	1151.47
Crystal system	triclinic
Space group	P -1
a/Å	13.75640(1)
b/Å	17.46850(1)
c/Å	25.0576(2)
α/deg	86.190(1)
β/deg	81.914(1)
γ/deg	67.772(1)
Volume/Å^3	5517.96(8)
Z	4
*D*calc /gcm^{-3}	1.386
μ(Mo-Kα)/mm^{-1}	3.630
F(000)	2352.0
Temperature/K	105(8)
λ/Å	1.54184
θ min, max/deg	3.748 / 79.497
Total, unique data	23561, 21874
R1(obsd/all) [a]	0.0670 / 0.0699
wR2(obsd/all) [b]	0.1888 / 0.1859
Goodness-of-fit on F^2	1.026

[a] $R = \sum||F_O| - |F_C||/\sum|F_O|$. [b] $Rw = [\sum \omega(|F_O| - |F_C|)2 / \sum \omega F_O]^{1/2}$.

Table S2 Selected bond lengths (Å) and angles (°) for **Ru^{IV}-*m*CPBA**[PF_6]·0.5C_3H_6O.

Ru1–O1	2.004(3)	O1–Ru1–N3	84.6(1)
Ru1–O2	2.034(3)	O1–Ru1–N4	92.9(1)
Ru1–O3	2.072(2)	O2–Ru1–O3	68.5(1)
Ru1–N1	2.104(3)	O2–Ru1–N1	137.3(1)
Ru1–N2	2.098(3)	O2–Ru1–N2	71.1(1)
Ru1–N3	2.143(3)	O2–Ru1–N3	104.5(1)
Ru1–N4	2.090(3)	O2–Ru1–N4	77.1(1)
O1–C24	1.408(5)	O3–Ru1–N1	151.8(1)
O2–C11	1.413(4)	O3–Ru1–N2	135.0(1)
O3–O4	1.437(4)	O1–Ru1–N3	88.4(1)
O4–C49	1.346(5)	O3–Ru1–N4	90.2(1)
O5–O49	1.203(6)	N1–Ru1–N2	73.0(1)
		N1–Ru1–N3	93.4(1)
O1–Ru1–O2	145.3(1)	N1–Ru1–N4	86.7(1)
O1–Ru1–O3	78.6(1)	N2–Ru1–N3	83.2(1)
O1–Ru1–N1	73.6(1)	N2–Ru1–N4	99.4(1)
O1–Ru1–N2	143.6(1)	N3–Ru1–N4	177.3(1)

Table S3 Yields of products in the oxidation of various substrates by **Ru^{III}** and H*m*CPBA.[a]

Entry	Substrate	Products (yield)
1	xanthene (20 mM)	xanthone (16%)
2	DHA (20 mM)	anthracene (15%) anthraquinone (7%) anthrone (13%)
3	fluorene (50 mM)	9-fluorenone (13%)
4	cumene (200 mM)	2-Phenyl-2-propanol (6%) acetophenone (9%)
5	ethylbenzene (200 mM)	1-phenylethanol (2%) acetophenone (3%)
6	toluene (500 mM)	benzaldehyde (2%) benzyl alcohol (1%)
7	cyclooctane (500 mM)	cyclooctanol (3%) cyclooctanone (1%)
8	cyclohexane (500 mM)	cyclohexanol (2%) cyclohexanone (1%)
9	thioanisole (20 mM)	methyl phenyl sulfoxide (33%) methyl phenyl sulfone (1%)
10	cyclohexene (50mM)	2-cyclohexen-1-ol (40%) cyclohexene oxide (1%)
11	styrene (50mM)	benzaldehyde (9%) styrene oxide (1%)
12	*cis*-1,2-dimethylcyclohexane (500 mM)	*cis*-1,2-dimethylcyclohexanol (3%) *trans*-1,2-dimethylcyclohexanol (1%)
13	xanthene (20 mM) (with 10 equiv. of Na_2SO_3)	xanthone (15%)
14	xanthene (20 mM) (with 10 equiv. of PPh_3)	xanthone (17%)
15	fluorene (50 mM) (with 10 equiv. of Na_2SO_3)	9-fluorenone (19%)
16	ethylbenzene (200 mM) (with 10 equiv. of Na_2SO_3)	1-phenylethanol (2%) acetophenone (4%)
17	cyclohexane (500 mM) (with 10 equiv. of Na_2SO_3)	cyclohexanol (2%) cyclohexanone (3%)

[a] **Ru^{III}** (1 mM) + H*m*CPBA (1 mM) in acetone under argon at 20 °C; yield was calculated based on **Ru^{III}**.

Table S4 Rate constants for the reaction between **Ru^{IV}-*m*CPBA** and hydrocarbons in acetone at 10 °C under Ar.

Hydrocarbons	**C–H BDEs / kcal mol^{-1}** [a]	**k_2 / M^{-1} s^{-1}**	**k_2' / M^{-1} s^{-1}** [b]
Xanthene	75.2	$(8.87 \pm 0.45) \times 10^{-2}$	$(4.44 \pm 0.23) \times 10^{-2}$
		$(2.27 \pm 0.17) \times 10^{-2}$ [c]	
DHA	78.0	$(8.44 \pm 0.12) \times 10^{-2}$	$(2.11 \pm 0.030) \times 10^{-2}$
		$(2.18 \pm 0.048) \times 10^{-2}$ [d]	
Fluorene	82.2	$(1.17 \pm 0.18) \times 10^{-2}$	$(5.85 \pm 0.90) \times 10^{-3}$
Cumene	84.5	$(2.59 \pm 0.15) \times 10^{-3}$	$(2.59 \pm 0.15) \times 10^{-3}$
Ethylbenzene	85.4	$(1.40 \pm 0.14) \times 10^{-3}$	$(7.00 \pm 0.70) \times 10^{-4}$
Toluene	89.7	$(5.70 \pm 0.57) \times 10^{-4}$	$(1.90 \pm 0.19) \times 10^{-4}$
Cyclooctane	95.7	$(1.56 \pm 0.085) \times 10^{-3}$	$(9.75 \pm 0.053) \times 10^{-5}$
Cyclohexane	99.5	$(3.99 \pm 0.22) \times 10^{-4}$	$(3.33 \pm 0.18) \times 10^{-5}$

[a] Data are from ref. 1. [b] k_2' = second-order rate constant per active hydrogen. [c] Xanthene-d_2 was used. [d] DHA-d_4 were used.

[1] (a) Parker, V. D. *J. Am. Chem. Soc.* **1992**, *114*, 7458-7462. (b) Bordwell, F. G.; Cheng, J. P.; Ji, G. Z.; Satish, A. V.; Zhang, X. J. *J. Am. Chem. Soc*. **1991**, *113*, 9790-9795. (c) *CRC Handbook of Chemistry and Physics, 82nd ed.*; Lide, D. R. Ed.; CRC Press: Boca Raton, 2001. (d) Luo, Y. R. *Handbook of Bond Dissociation Energies in Organic Compounds*, CRC Press: Boca Raton, 2003.

Table S5 Yields of by-products in the oxidation of various substrates.

Entry	**Substrate**	**Products (yield %)**	
		chlorobenzene	**m-chlorobenzoic acid**
1[a]	xanthene	4	91
2[b]	xanthene	3	85
3[a]	DHA	7	80
4[b]	DHA	2	89

[a] **Ru^{III}** (1 mM) + H*m*CPBA (1 mM) in acetone under argon at 20.0 °C; yield was calculated based on **Ru^{III}**.

[b] H*m*CPBA (1 mM) in acetone under argon at 20.0 °C; yield was calculated based on H*m*CPBA.

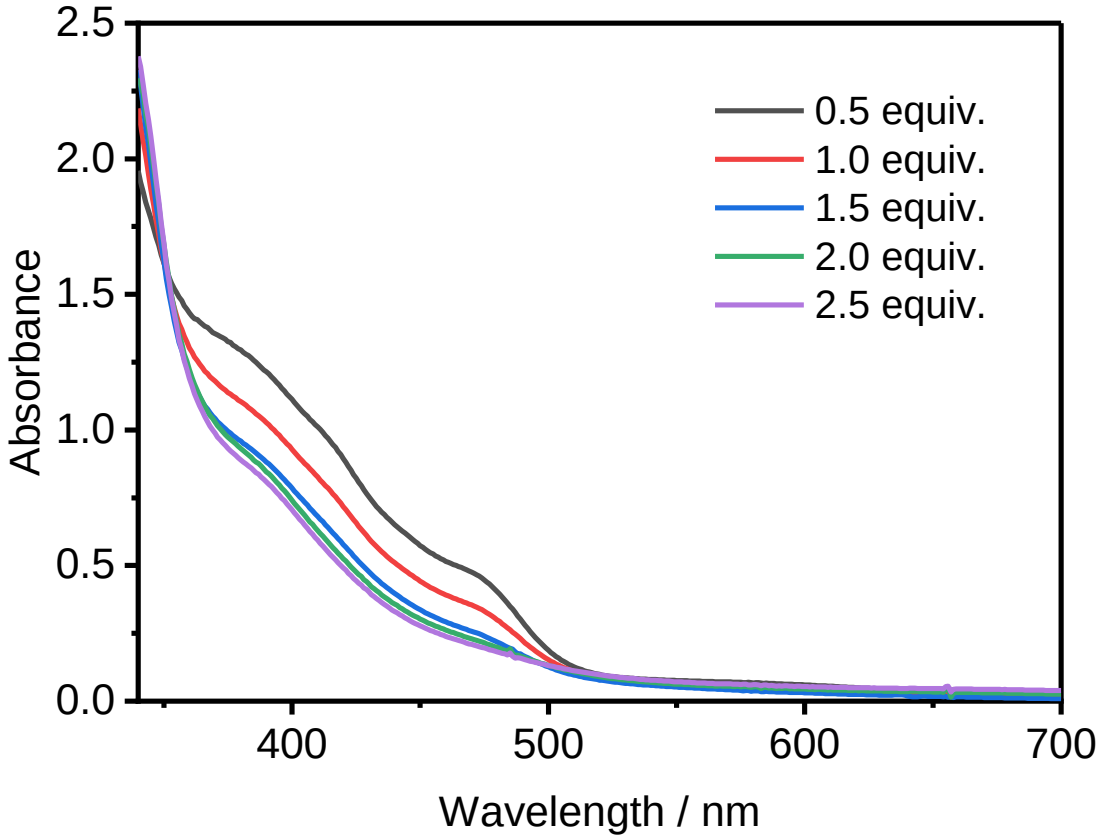

Figure S1 UV-Vis spectral titrations which was carried out using various amount of H*m*CPBA and **Ru^{III}** (3.00×10^{-4} M) in acetone at 0 °C under Ar. Spectra are picked where the absorbance at 472 nm reaches the minimum.

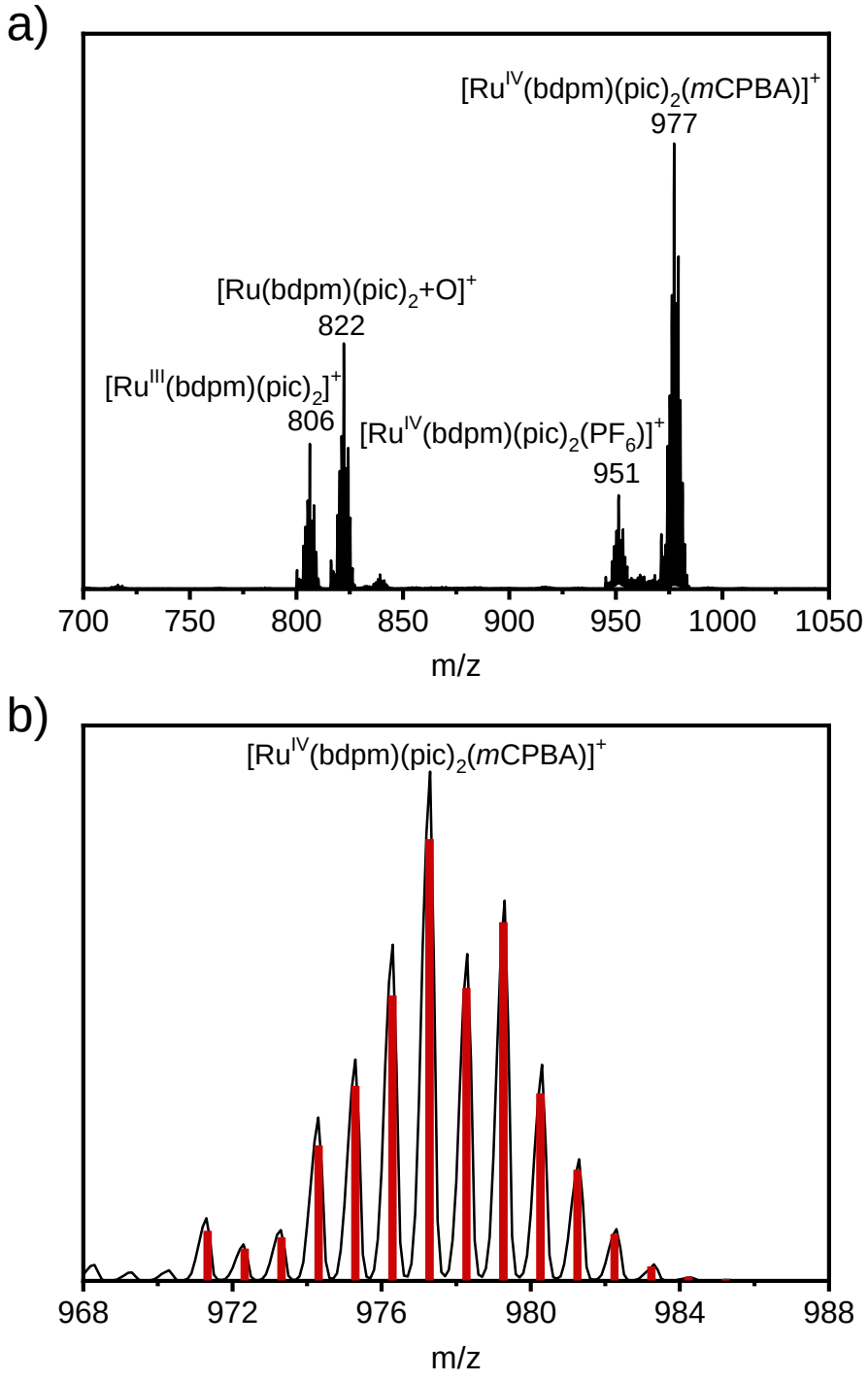

Figure S2 a) ESI/MS of the in situ generated **Ru^{IV}-*m*CPBA** (1 mM) in acetone; b) expanded (black line) and calculated (red bar) isotopic patterns of **Ru^{IV}-*m*CPBA**.

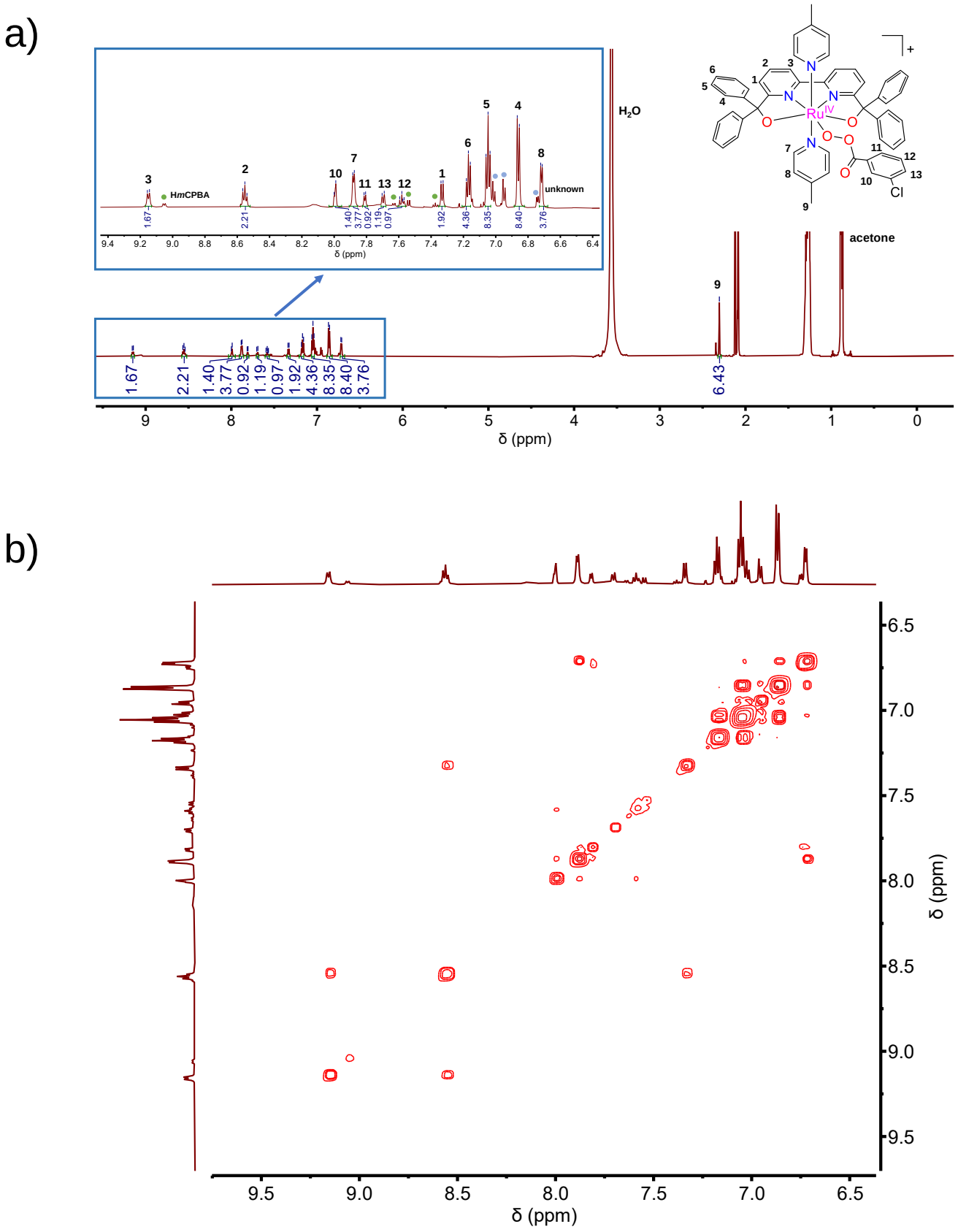

Figure S3 ^{1}H NMR of isolated **Ru^{IV}-*m*CPBA** in acetone-d_6 at −20 °C.

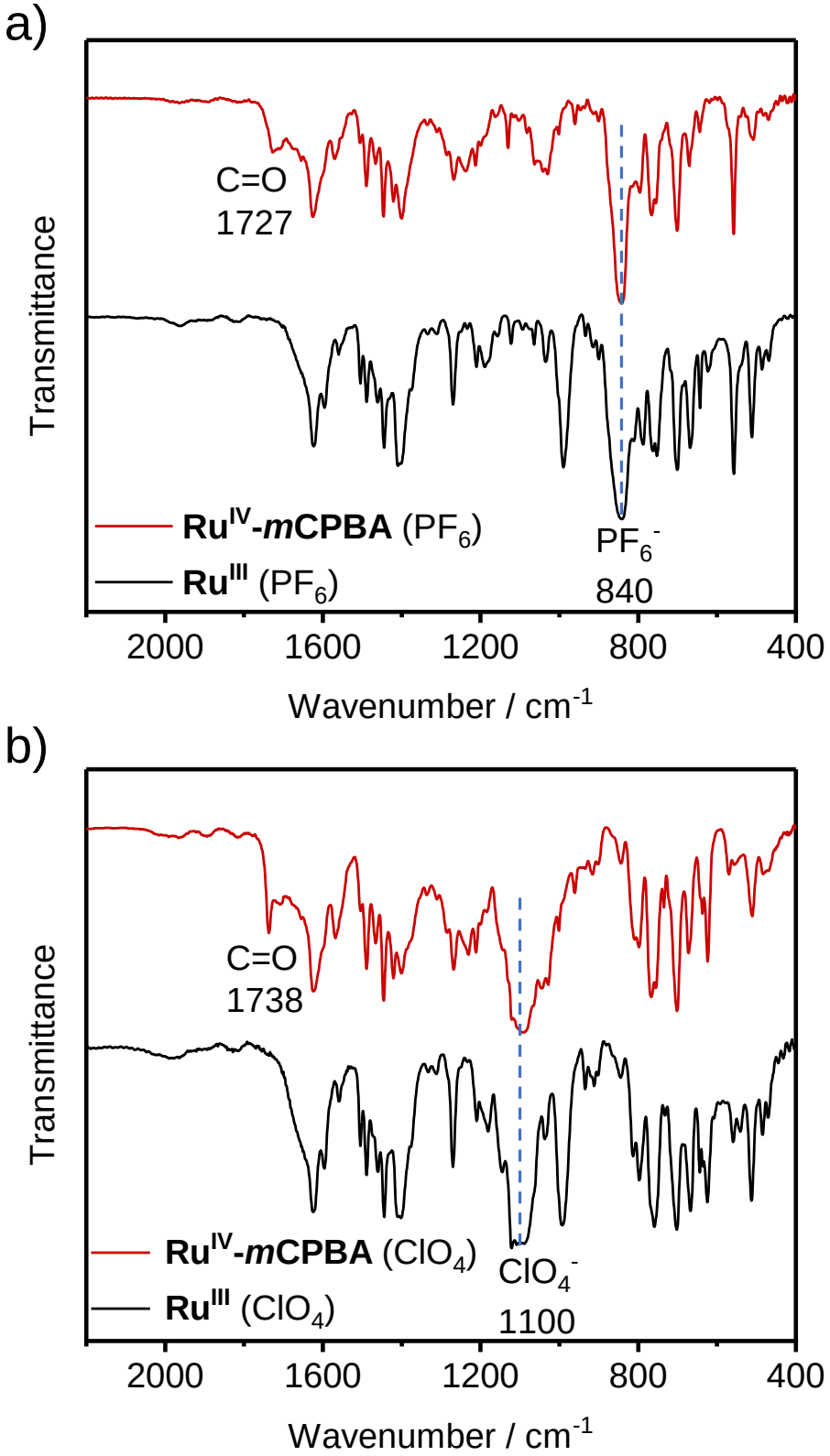

Figure S4 IR spectra of **Ru^{III}** and the isolated solid **Ru^{IV}-*m*CPBA**. a) samples prepared using PF_6^- salt; b) samples prepared using ClO_4^- salt. The O−O bond stretching usually occurs in the range of 780-880 cm^{-1}. No obvious peaks belong to O−O bond stretching can be observed in this region.

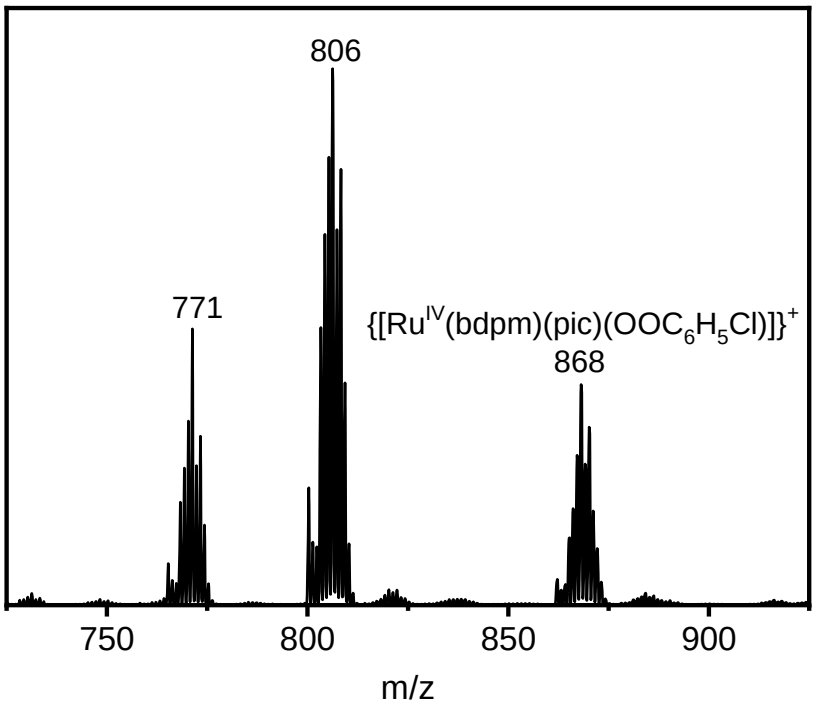

Figure S5 ESI/MS of the isolated solid state **Ru^{IV}-*m*CPBA** at 20 ℃ after 30 min. The sample was prepared by dissolving solid sample in acetone.

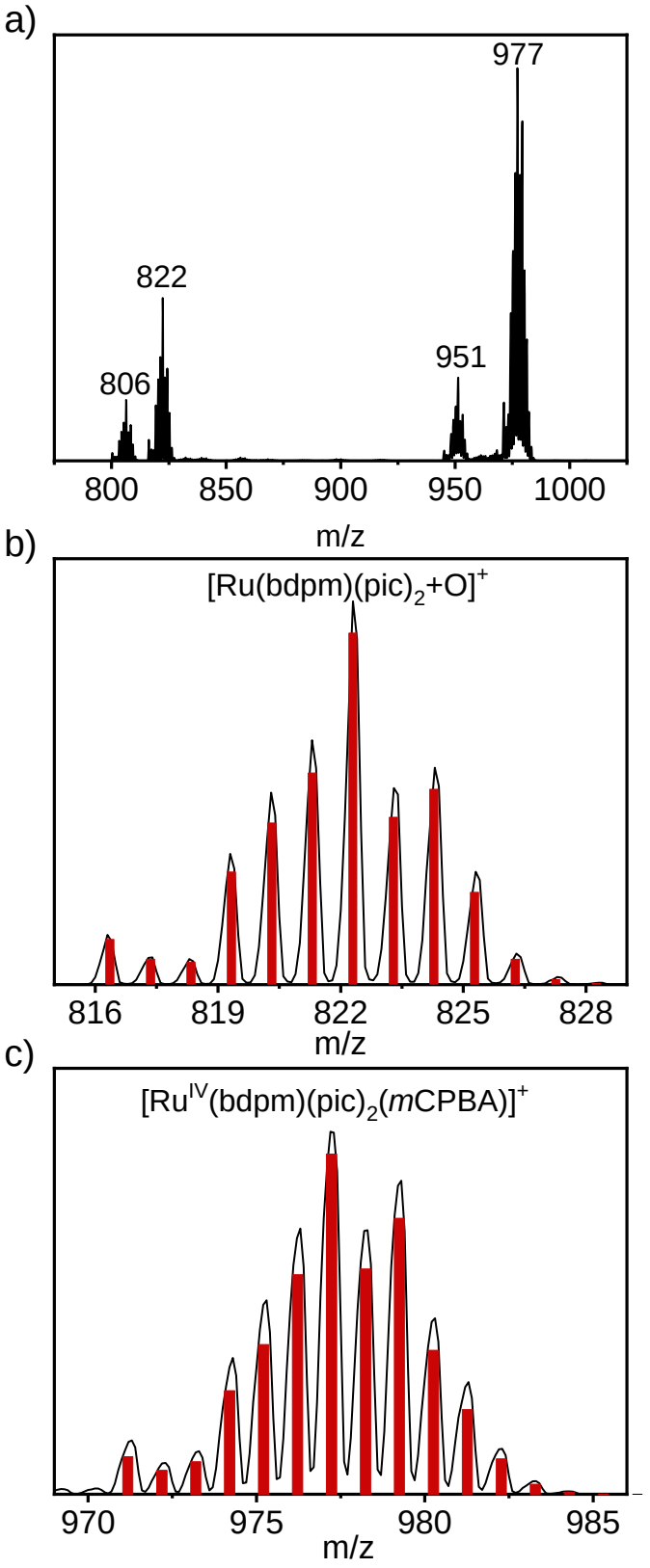

Figure S6 a) ESI/MS of **Ru^{IV}-*m*CPBA** (1 mM, in acetone) in the presence of $H_2{}^{18}O$ (40 μL); b) and c) are expanded (black line) and calculated (red bar) isotopic patterns of Ru species. No ^{18}O-labelled peaks were found.

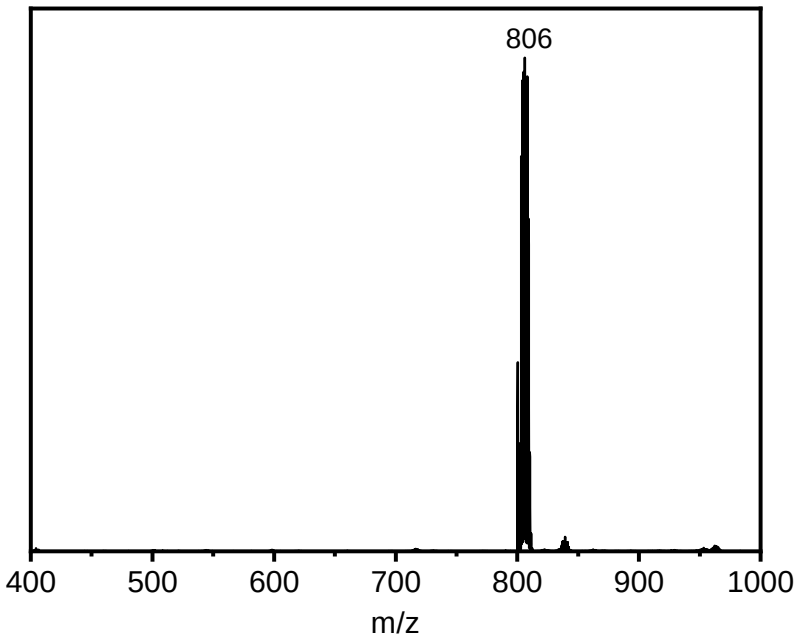

Figure S7 ESI/MS of the reaction of in situ generated **Ru^{IV}-*m*CPBA** (1 mM) and DHA (20 mM) in acetone after 2h.

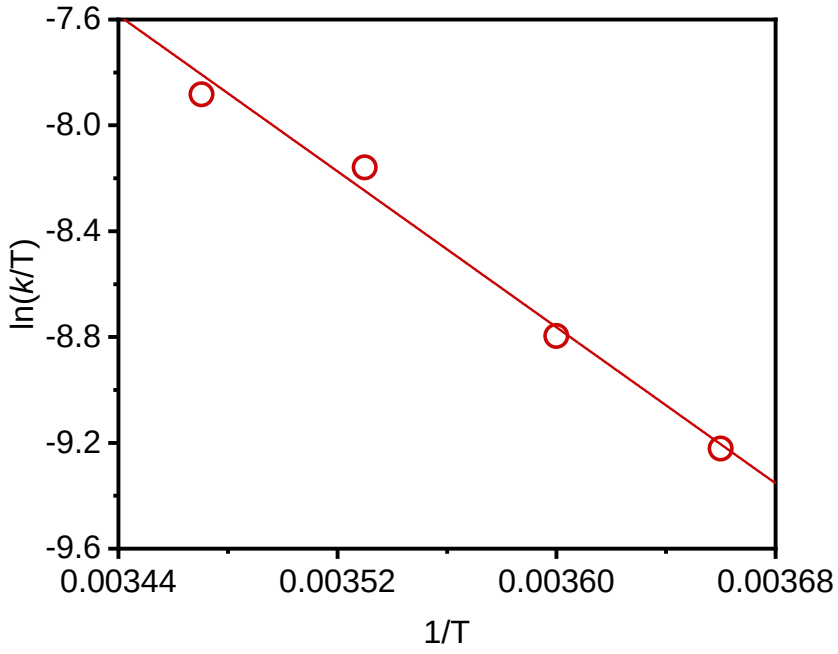

Figure S8 Eyring plot for the reaction of the in situ generated **Ru^{IV}-*m*CPBA** and DHA in acetone. Slope = −(7370.8 ± 739.1), y-intersept = (17.8 ± 2.6), $\triangle H^{\ddagger}$ = 14.7 ± 1.4 kcal mol^{-1} and $\triangle S^{\ddagger}$ = −11.9 ± 5.1 cal mol^{-1} K^{-1}.

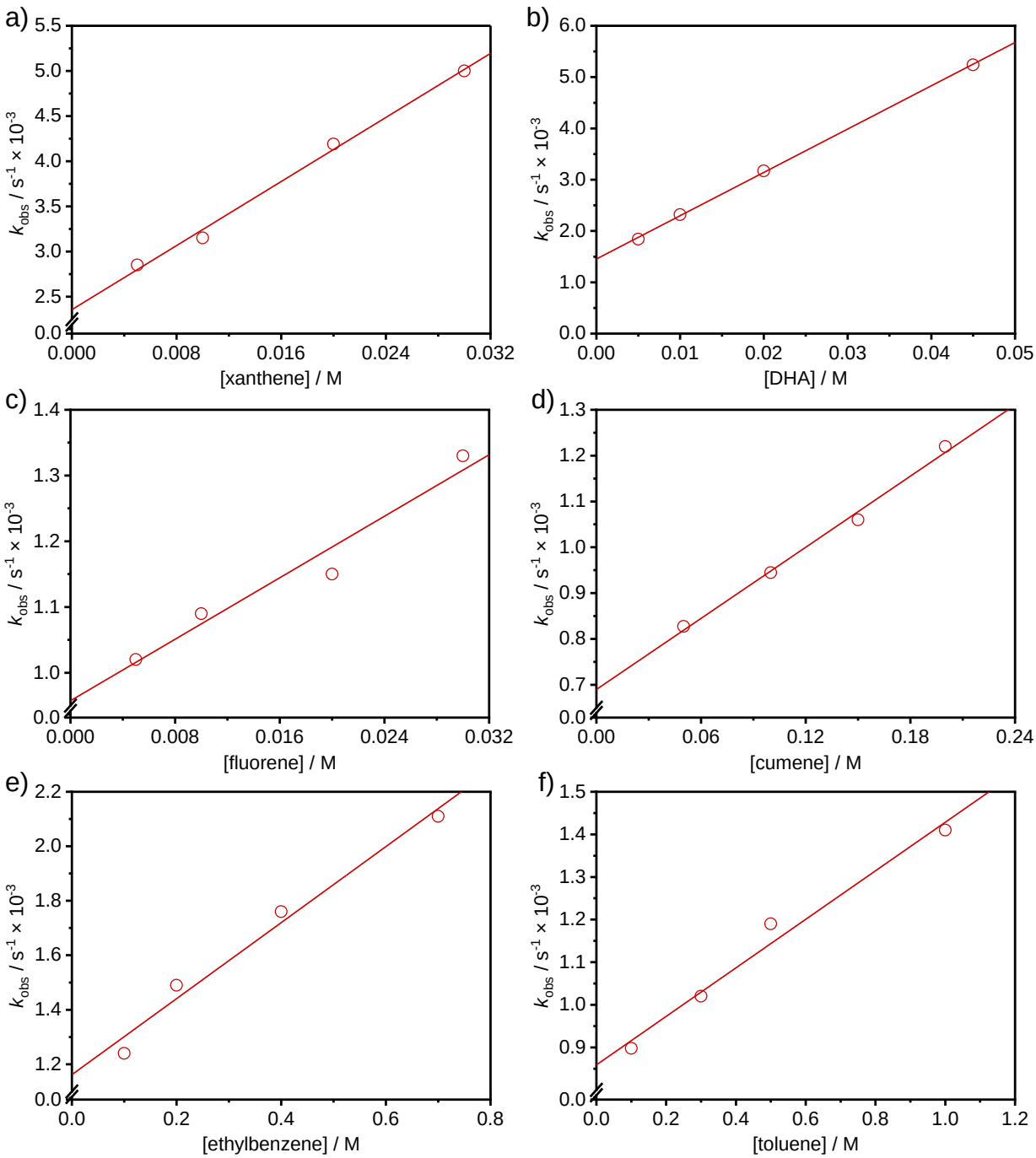
a)
k_{obs} / s^{-1} × 10^{-3}
[xanthene] / M
b)
k_{obs} / s^{-1} × 10^{-3}
[DHA] / M
c)
k_{obs} / s^{-1} × 10^{-3}
[fluorene] / M
d)
k_{obs} / s^{-1} × 10^{-3}
[cumene] / M
e)
k_{obs} / s^{-1} × 10^{-3}
[ethylbenzene] / M
f)
k_{obs} / s^{-1} × 10^{-3}
[toluene] / M

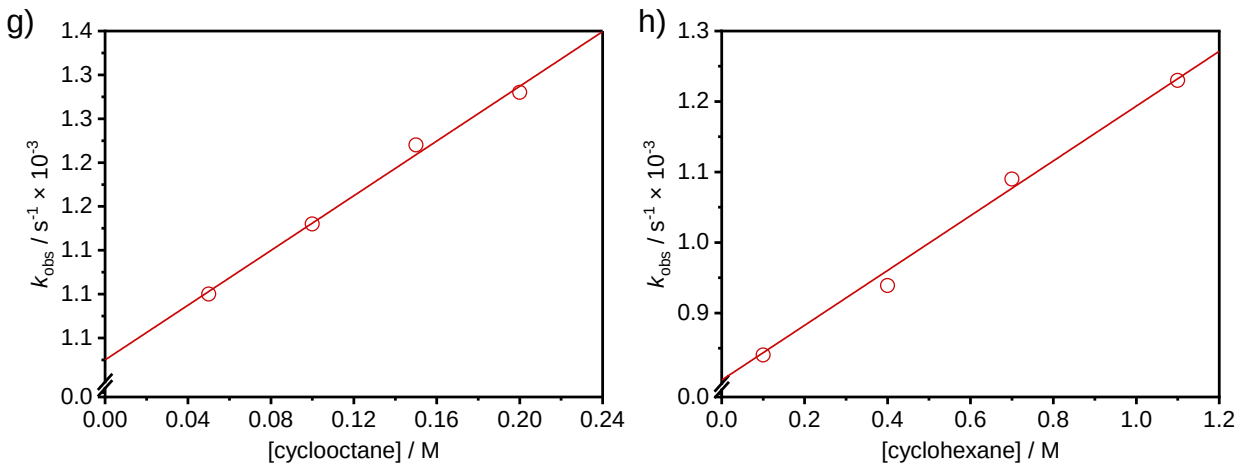

Figure S9 Plot of k_{obs} against [substrates] at 10 °C. a) xanthene: slope = (8.87 ± 0.45) × 10^{-2}, y-intercept = (2.36 ± 0.085) × 10^{-3}, r^2 = 0.992; b) DHA: slope = (8.44 ± 0.12) × 10^{-2}, y-intercept = (1.45 ± 0.030) × 10^{-3}, r^2 = 0.999; c) fluorene: slope = (1.17 ± 0.18) × 10^{-2}, y-intercept = (9.58 ± 0.34) × 10^{-4}, r^2 = 0.931; d) cumene: slope = (2.59 ± 0.15) × 10^{-3}, y-intercept = (6.70 ± 0.21) × 10^{-4}, r^2 = 0.990; e) ethylbenzene: slope = (1.40 ± 0.14) × 10^{-3}, y-intercept = (1.16 ± 0.060) × 10^{-3}, r^2 = 0.969; f) toluene: slope = (5.70 ± 0.57) × 10^{-4}, y-intercept = (8.59 ± 0.33) × 10^{-4}, r^2 = 0.970; g) cyclooctane: slope = (1.56 ± 0.085) × 10^{-3}, y-intercept = (1.03 ± 0.12) × 10^{-3}, r^2 = 0.991; h) cyclohexane: slope = (3.89 ± 0.15) × 10^{-4}, y-intercept = (8.05 ± 0.086) × 10^{-4}, r^2 = 0.992.

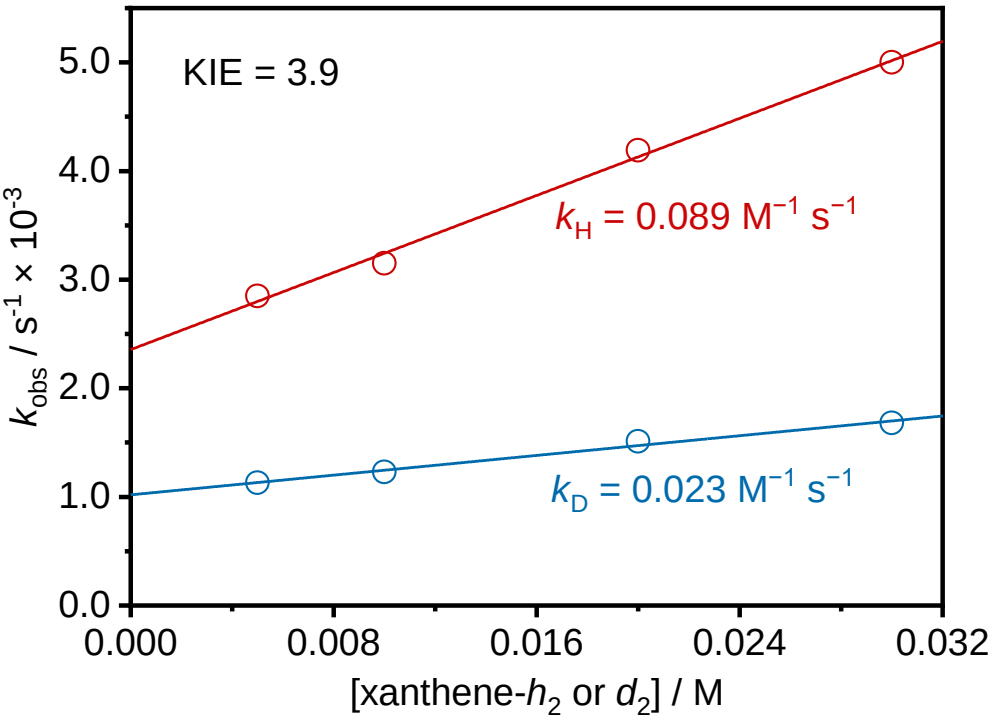

Figure S10 Plot of k_{obs} against xanthene at 10 °C: slope = (0.089 ± 0.005), r^2 = 0.992; xanthene-d_2: slope = (0.023 ± 0.002), r^2 = 0.984; KIE = (3.9 ± 0.6).

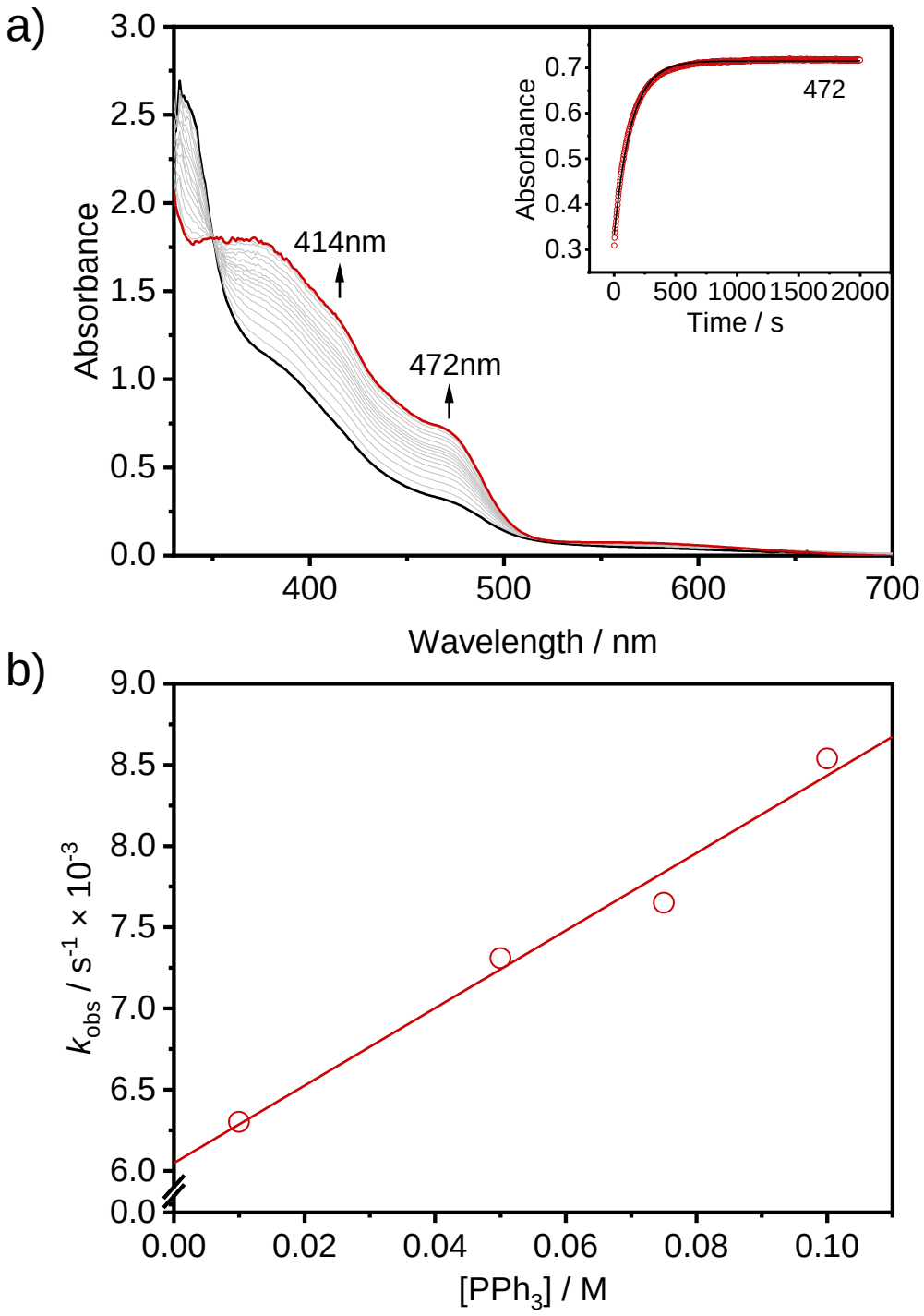

Figure S11 a) UV-Vis spectral changes of reaction between the in situ generated **Ru^{IV}-*m*CPBA** (3.00×10^{-4} M) and PPh_3 (0.05 M) in acetone at –10 °C under Ar. Inset shows the corresponding absorbance-time trace at 472 nm. b) Plot of k_{obs} against the concentrations of PPh_3. [slope = $(2.39 \pm 0.24) \times 10^{-2}$, y-intercept = $(6.05 \pm 0.16) \times 10^{-3}$, $r^2 = 0.970$.]

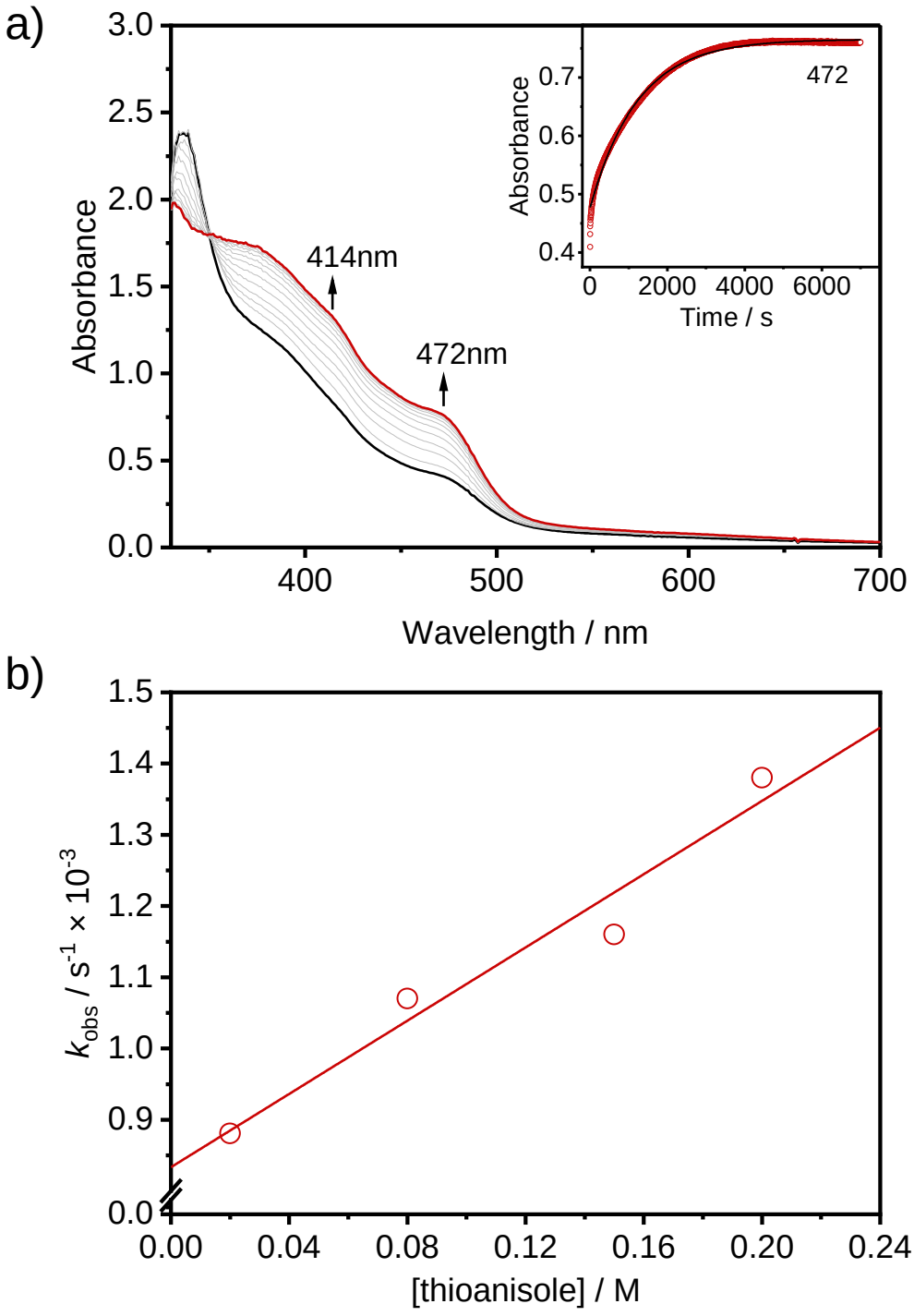

Figure S12 a) UV-Vis spectral changes of reaction between the in situ generated **Ru^{IV}-*m*CPBA** (3.00×10^{-4} M) and thioanisole (0.02 M) in acetone at 0 °C under Ar. Inset shows the corresponding absorbance-time trace at 472 nm. b) Plot of k_{obs} against the concentrations of thioanisole. [slope = $(2.57 \pm 0.38) \times 10^{-3}$, y-intercept = $(8.33 \pm 0.51) \times 10^{-4}$, $r^2 = 0.940$.]

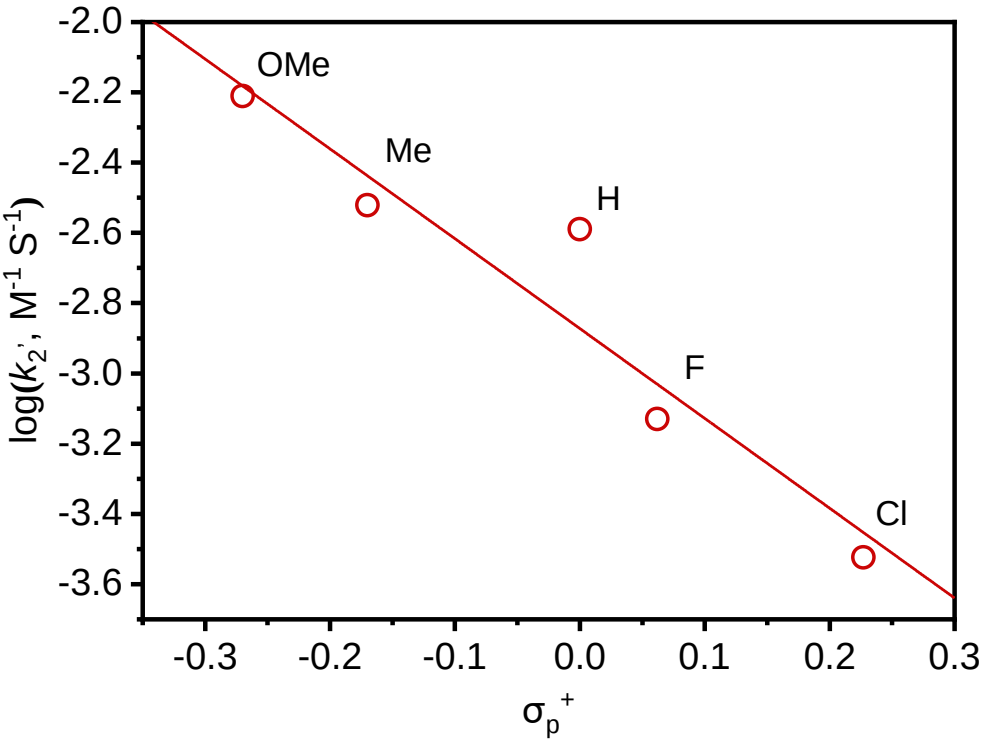

Figure S13 Hammett plot for the reaction of the in situ generated **Ru^{IV}-*m*CPBA** (3.00×10^{-4} M) and different para-substituted thioanisoles in acetone at 0 °C under Ar. [slope = – (2.56 ± 0.47), y-intercept = – (2.87 ± 0.084), r^2=0.876.]

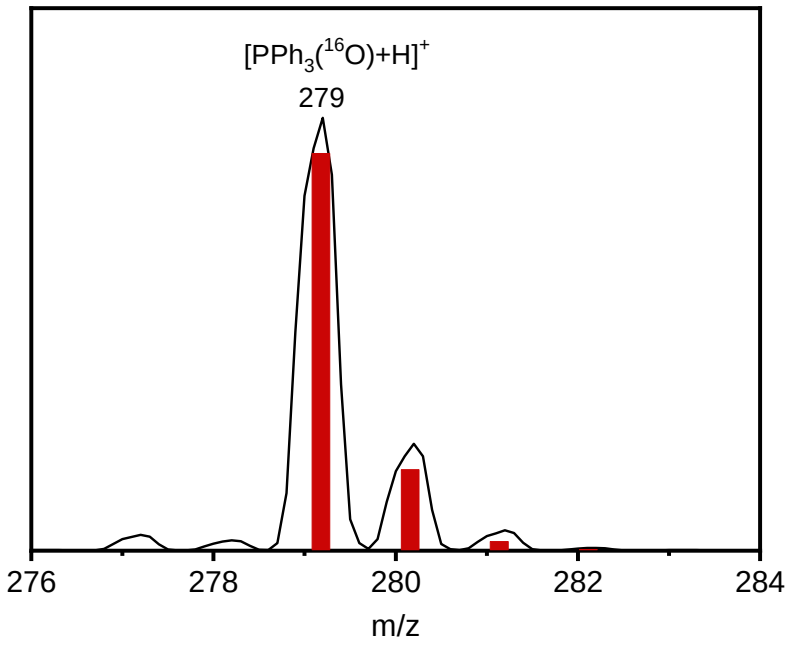

Figure S14 ESI/MS of reaction solution of **Ru^{IV}-*m*CPBA** (1 mM) and PPh_3 (50 mM) in the presence of $H_2{}^{18}O$ (40 μL) in acetone. Red bar is calculated isotopic pattern.

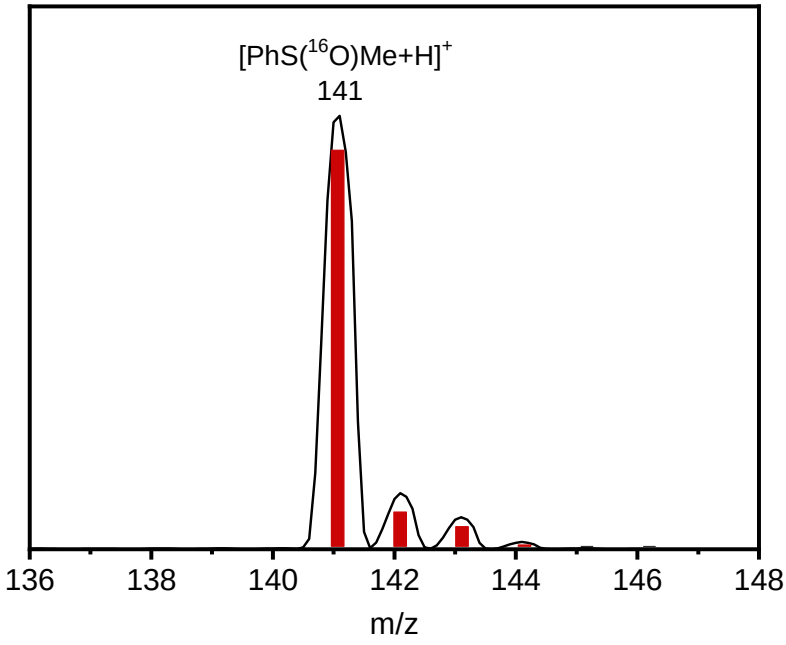

Figure S15 ESI/MS of reaction solution of **Ru^{IV}-*m*CPBA** (1 mM) and thioanisole (20 mM) in the presence of $H_2{}^{18}O$ (40 μL) in acetone. Red bar is calculated isotopic pattern.

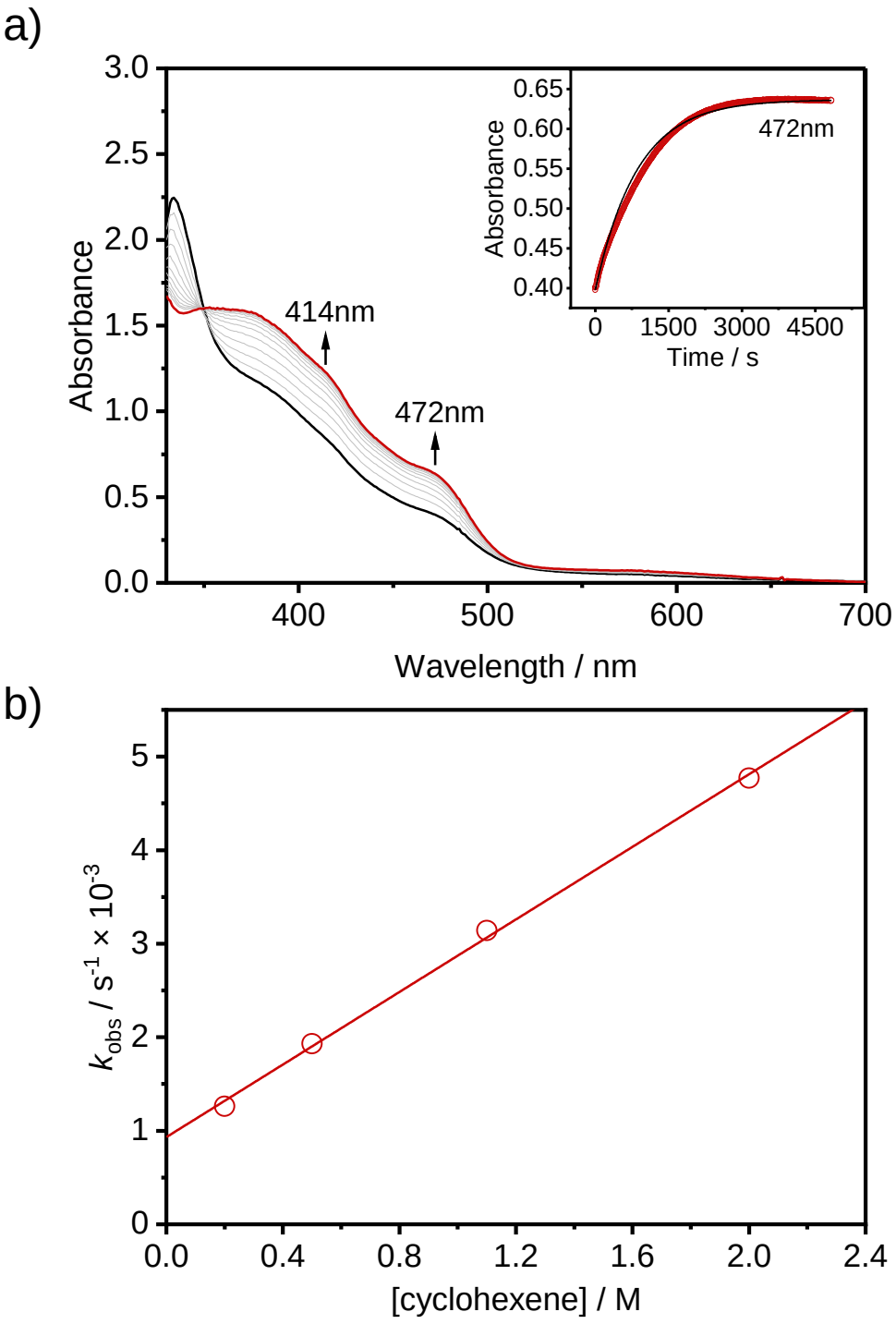

Figure S16 a) UV-Vis spectral changes of reaction between the in situ generated **Ru^{IV}-*m*CPBA** (3.00×10^{-4} M) and cyclohexene (0.2 M) in acetone at 0 °C under Ar. Inset shows the corresponding absorbance-time trace at 472 nm. b) Plot of k_{obs} against the concentrations of cyclohexene. [slope = $(1.94 \pm 0.06) \times 10^{-3}$, y-intercept = $(9.32 \pm 0.65) \times 10^{-4}$, $r^2 = 0.998$]

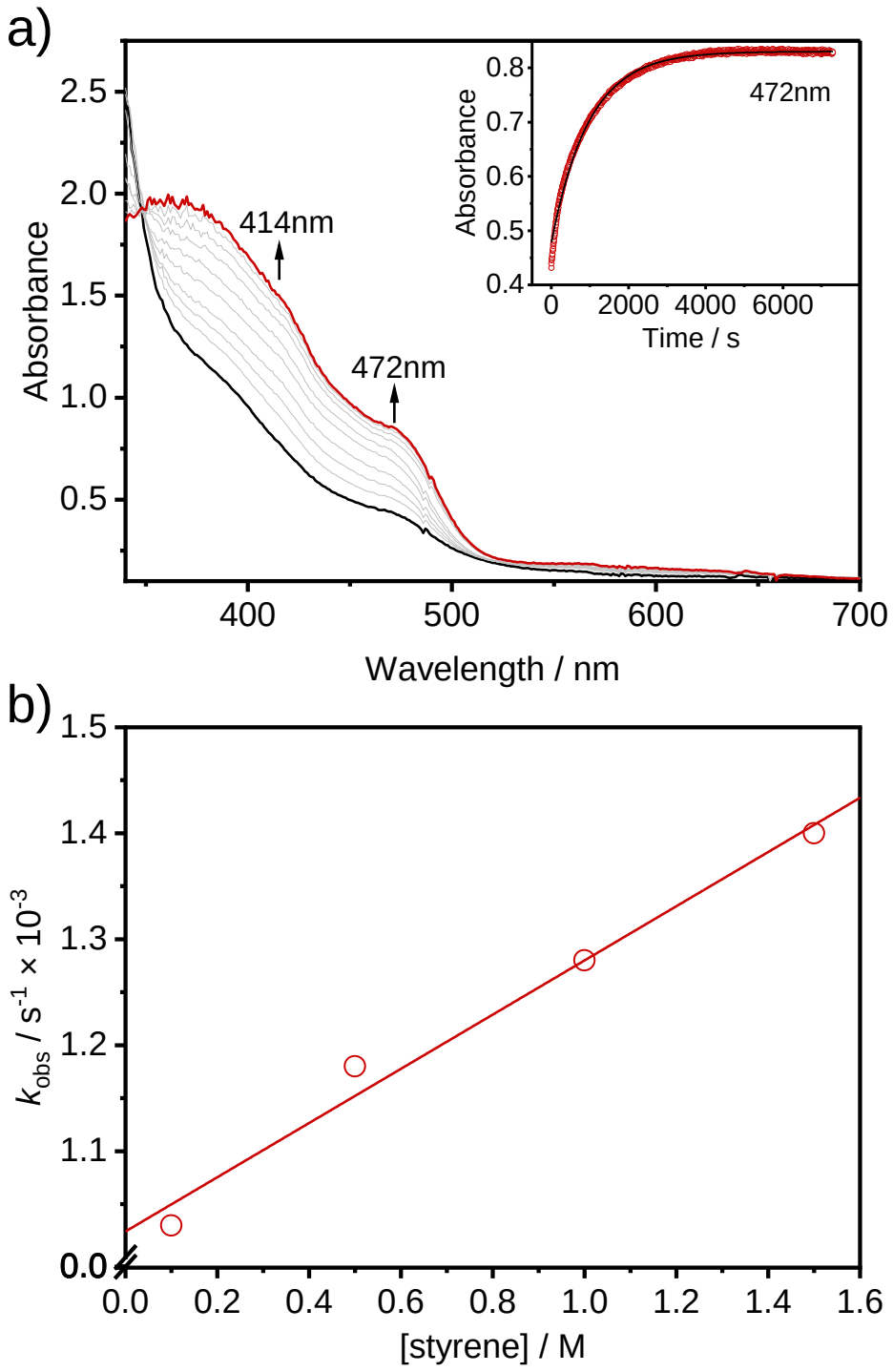

Figure S17 a) UV-Vis spectral changes of reaction between the in situ generated **Ru^{IV}-*m*CPBA** (1.00×10^{-3} M) and styrene (0.1 M) in acetone at 10 °C under Ar. Inset shows the corresponding absorbance-time trace at 472 nm. b) Plot of k_{obs} against the concentrations of styrene. [slope = $(2.56 \pm 0.24) \times 10^{-2}$, y-intercept = $(1.02 \pm 0.22) \times 10^{-3}$, $r^2 = 0.975$.]

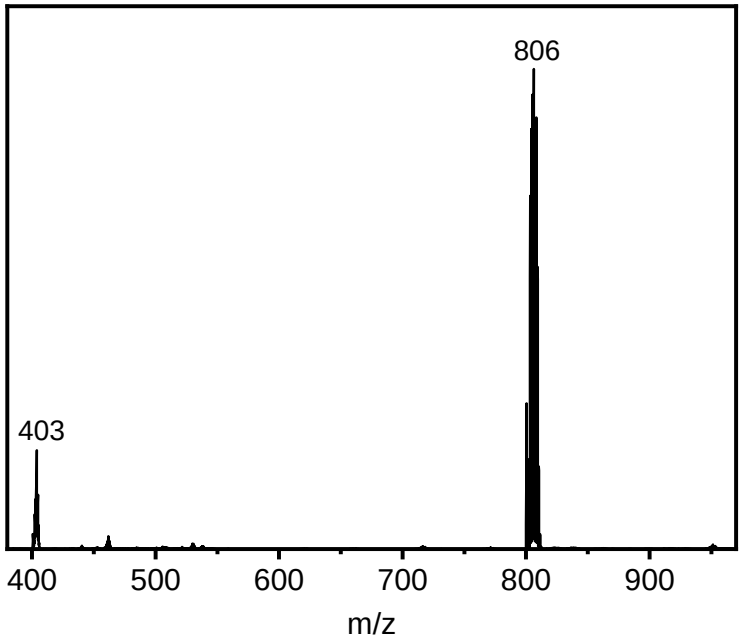

Figure S18 ESI/MS of the in situ generated **Ru^{IV}-*m*CPBA** (1 mM) and cyclohexene (20 mM) in acetone after 2h.

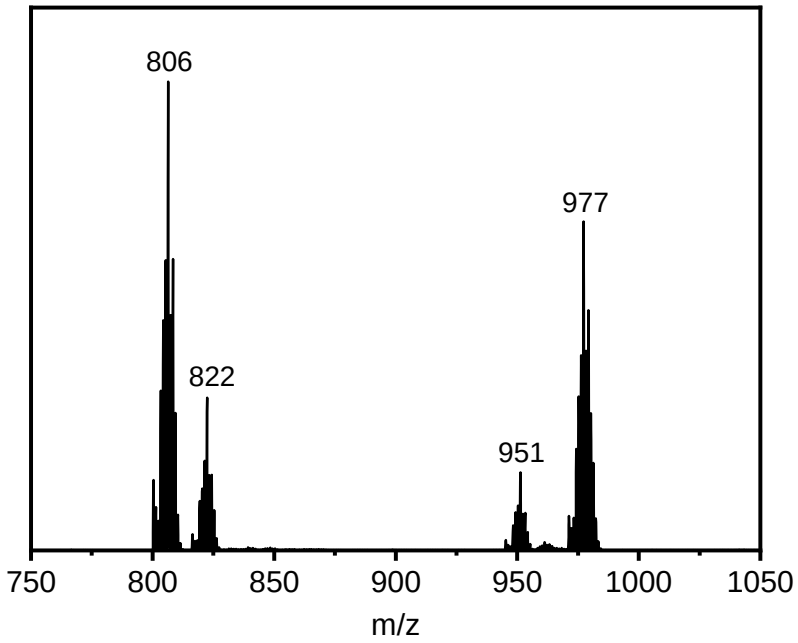

Figure S19 ESI/MS of the isolated **Ru^{IV}-*m*CPBA** in MeCN.

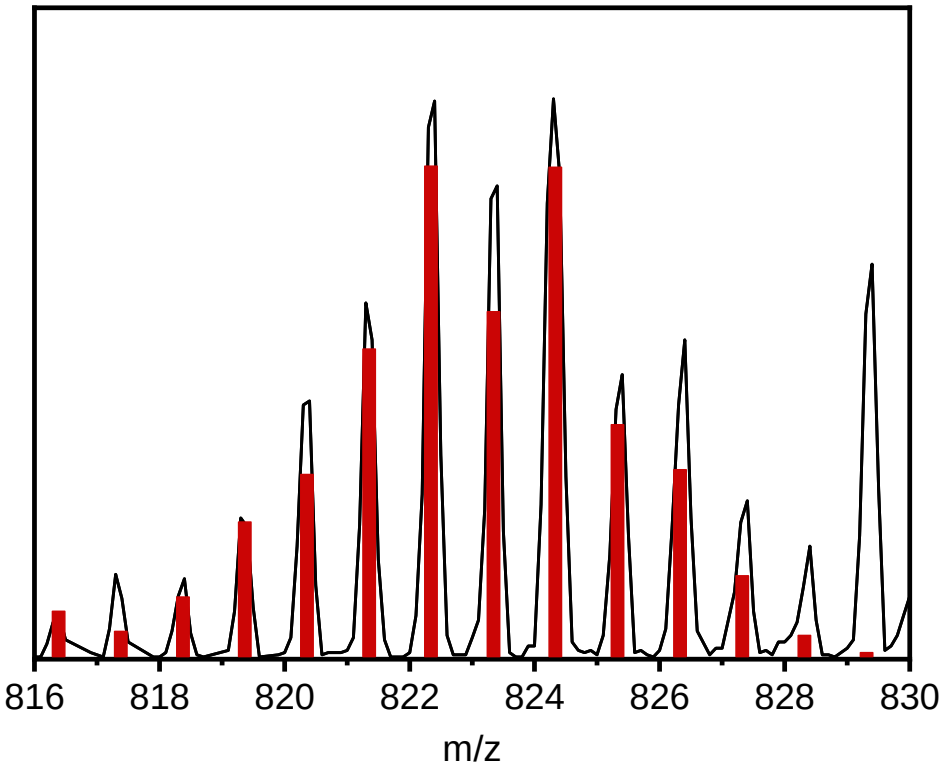

Figure S20 ESI/MS of reaction solution of **Ru^{III}** (1.5 mM) + Ce(IV) (3.0 mM) in the presence of $H_2{}^{18}O$ (40 μL) in acetone/H_2O (v:v 10:1). Calculated isotopic pattern (red bar) indicates that the species at *m*/*z* = 822 is 45% ^{18}O-enriched.

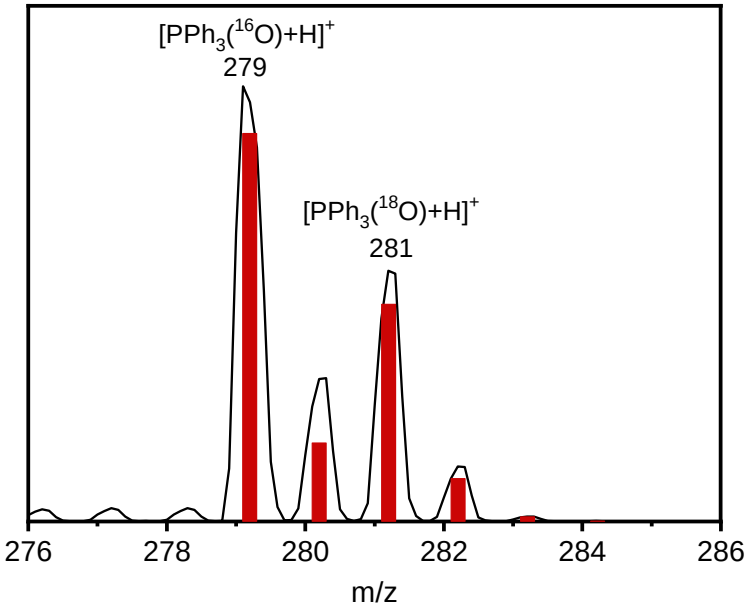

Figure S21 ESI/MS of reaction solution of **Ru^{III}** (1.5 mM) + Ce(IV) (3.0 mM) + PPh_3 (50 mM) in the presence of $H_2{}^{18}O$ (40 μL) in acetone. Calculated isotopic pattern (red bar) indicates **PPh_3O** is 35% ^{18}O-enriched.

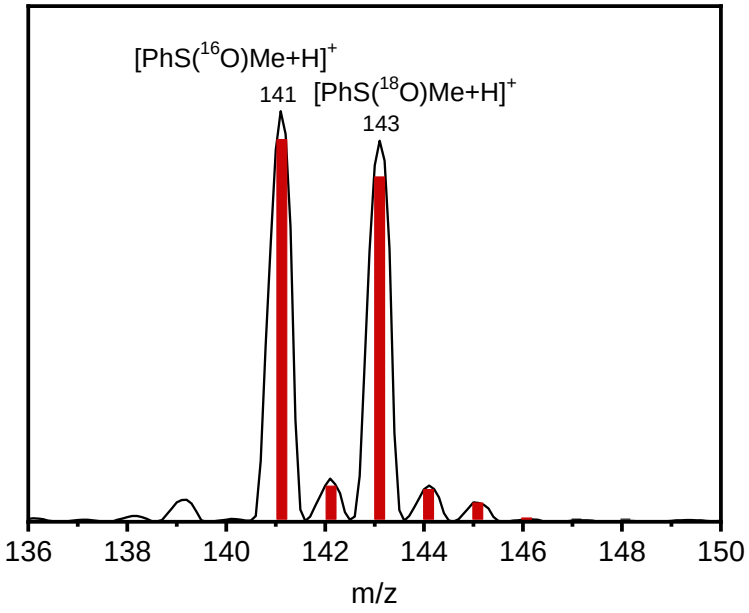

Figure S22 ESI/MS of reaction solution of **Ru^{III}** (1.5 mM) + Ce(IV) (3.0 mM) + thioanisloe (50 mM) in the presence of $H_2{}^{18}O$ (40 μL) in acetone. Calculated isotopic pattern (red bar) indicates methyl phenyl sulfoxide is 46% ^{18}O-enriched.

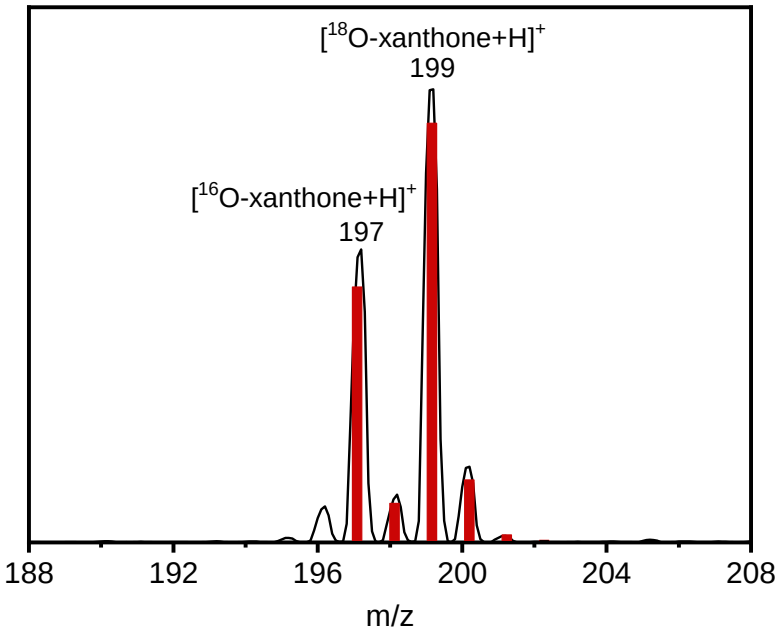

Figure S23 ESI/MS of reaction solution of **Ru^{III}** (1.5 mM) + Ce(IV) (3 mM) + xanthene (20 mM) in the presence of $H_2{}^{18}O$ (40 μL) in MeCN. Calculated isotopic pattern (red bar) indicates xanthene is 65% ^{18}O-enriched.

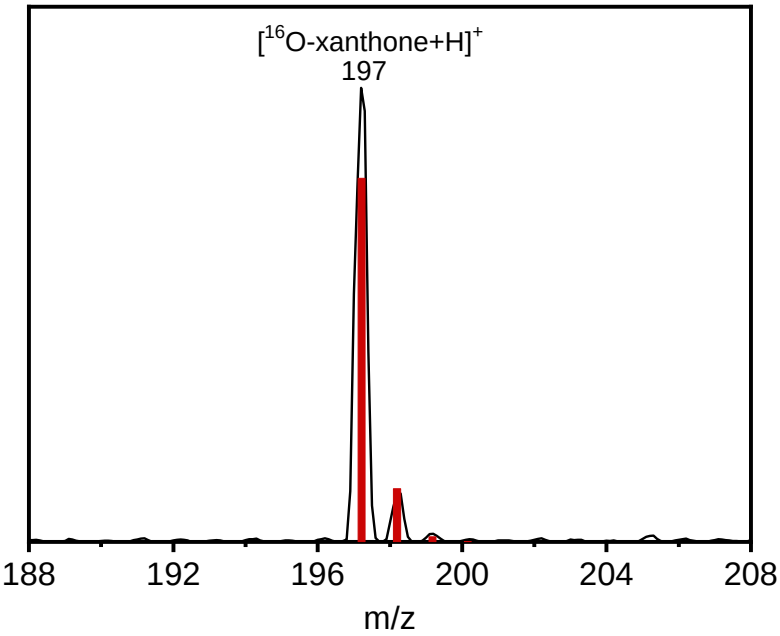

Figure S24 ESI/MS of reaction solution of **Ru^{IV}-*m*CPBA** (1 mM) and xanthene (20 mM) in the presence of $H_2{}^{18}O$ (40 μL) in acetone. Red bar is calculated isotopic pattern.

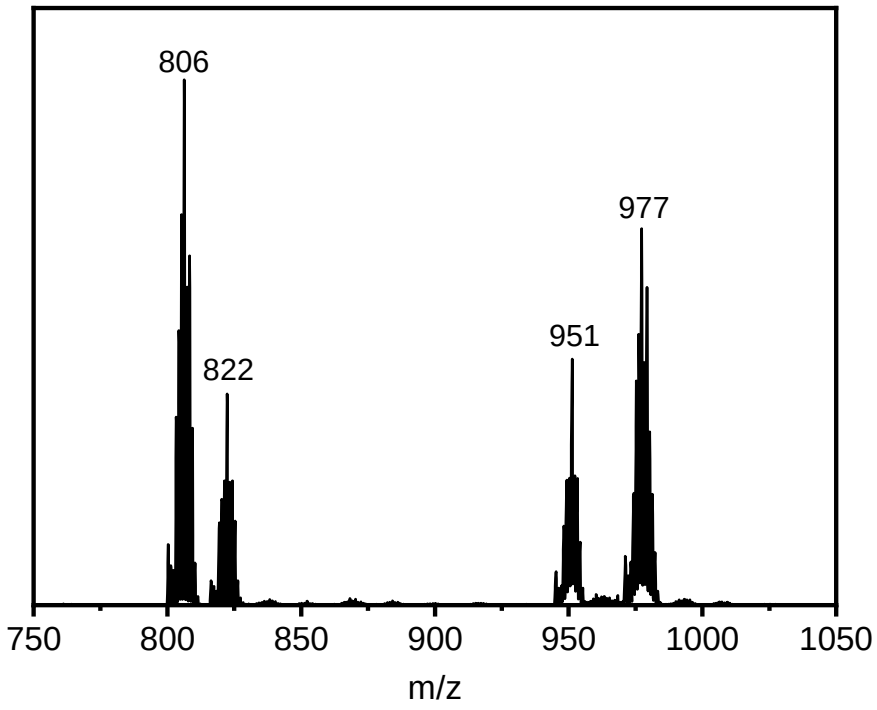

Figure S25 ESI/MS of the isolated solid **Ru^{IV}-*m*CPBA** in acetone.

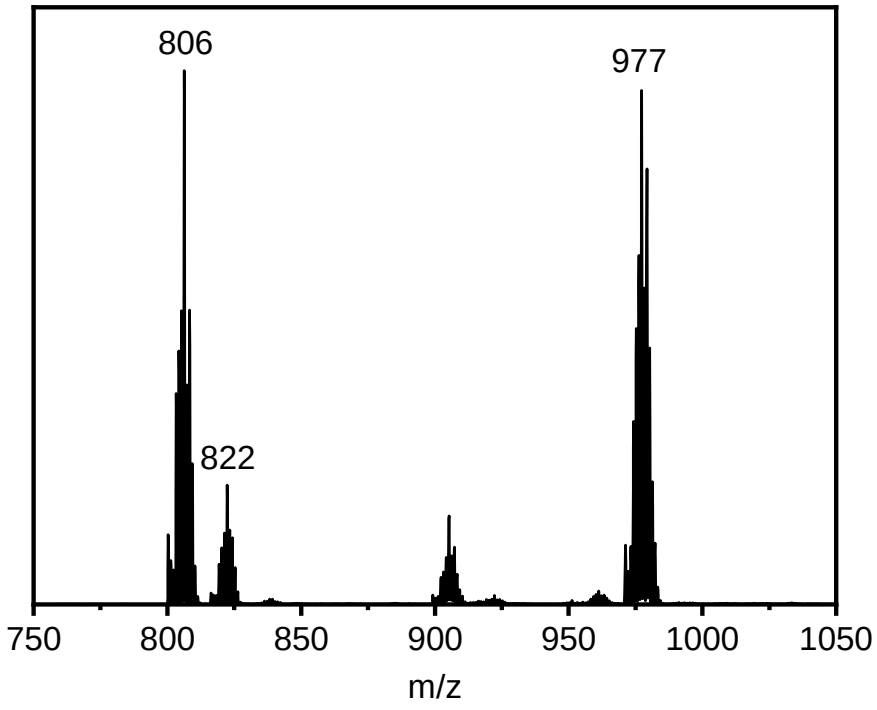

Figure S26 ESI/MS of the isolated solid **Ru^{IV}-*m*CPBA** (ClO_4) in acetone.

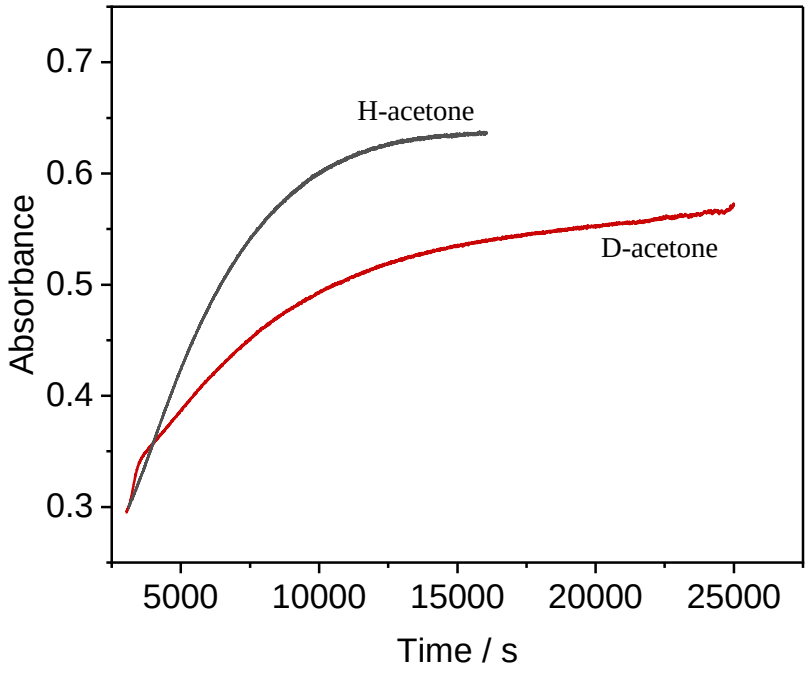

Figure S27 The corresponding absorbance-time trace of **Ru^{IV}-*m*CPBA** (3.00×10^{-4} M) in acetone and D-acetone at 472 nm at 0 °C under Ar.

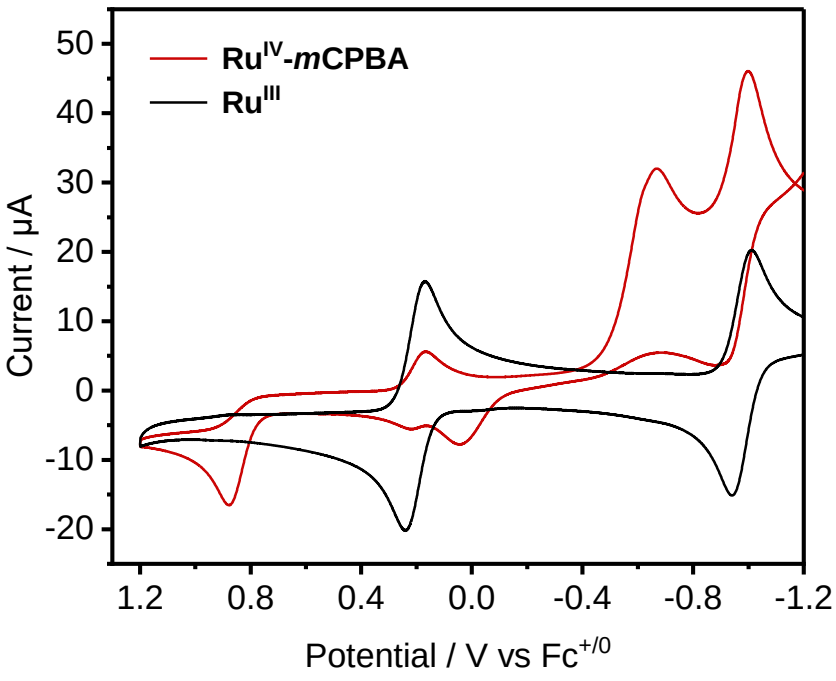

Figure S28 CVs of in situ generated **Ru^{IV}-*m*CPBA** and **Ru^{III}** (1 mM) in acetone (0.1 M $^{n}Bu_4NPF_6$) at 0 °C under argon. Scan rate = 100 mV s^{-1}.

References

[1] Amarego, W. L. F. *Purification of Laboratory Chemicals, 8th ed*.; Butterworth-Heinemann: Cambridge, **2017**.

[2] Gao, H.; Groves, J. T. Fast Hydrogen Atom Abstraction by a Hydroxo Iron(III) Porphyrazine. *J. Am. Chem. Soc.* **2017**, *139*, 3938–3941.

[3] Pan, Y.; Zhou, M.; Wang, R., Song, D., Yiu, S. M., Xie, J., Lau, K. C., Lau, T. C., Liu, Y.; Structure and Reactivity of a Seven-Coordinate Ruthenium Iodosylbenzene Complex. *Inorg. Chem.*, **2023**, *62*, 7772–7778.

[4] CrysAlisPro, Rigaku Oxford Diffraction, version 1.171.41.123a, 2022.

[5] SCALE3 ABSPACK – A Rigaku Oxford Diffraction program for Absorption Corrections, Rigaku Oxford Diffraction, **2017**.

[6] Sheldrick, G. M. SHELXT-Integrated Space-Group and Crystal-Structure Determination. *Acta Cryst.*, **2015**, *A71*, 3–8.

[7] Sheldrick, G. M. Crystal Structure Refinement with SHELXL. *Acta Cryst.* **2015**, *C71*, 3–8.

[8] Olex2 1.5 - compiled 2022.04.07 svn. rca3783a0 for OlexSys, GUI svn.r6498.

[9] Dolomanov, O. V.; Bourhis, L. J.; Gildea, R. J.; Howard, J. A. K.; Puschmann, H. OLEX2: A Complete Structure Solution, Refinement and Analysis Program. *J. Appl. Crystallogr.* **2009**, *42*, 339–341.

[10] Kratzert, D., Krossing, I. Recent improvements in DSR. *J. Appl. Crystallogr.*, **2018**. *51*, 928–934.